RECENT HEAVY FLAVOUR RESULTS FROM CMS*

Stefano Lacaprara

on behalf of the CMS Collaboration

Istituto Nazionale di Fisica Nucleare, Sezione di Padova
Via Marzolo 8, 35131 Padova, Italy

(Received April 20, 2018)

Recent results on b-flavour physics obtained by the CMS Collaboration will be presented. The flexible and powerful CMS trigger system allows the experiment to be sensitive to b-physics phenomena of different kinds, mostly in channels with muons in the final state. In this paper, some of these results will be reported, namely single quarkonia production, J/ψ, $\psi(2S)$, $\Upsilon(1S, 2S, 3S)$, as well as the observation of double prompt Υ production. The lifetimes of different states, $B^0 \to J/\psi K^\star$, $B^0 \to J/\psi K_{\rm S}$, $B_s^0 \to J/\psi\pi\pi$, $B_s^0 \to J/\psi\phi$, $\Lambda_b \to J/\psi\Lambda$, and $B_c^+ \to J/\psi\pi$ will be described. Other measurements include Λ_b polarization, search for $X^+(5568) \to B_s^0\pi^+$, and the rare decay $B_s^0 \to \mu\mu$. Finally, the recent measurements of some angular parameters of the $B^0 \to K^\star\mu\mu$ decay will be reviewed.

DOI:10.5506/APhysPolB.49.1199

1. Introduction

The CMS experiment [1] has been designed to allow a wide spectrum of physics measurements, both in the range of high transverse momentum ($p_{\rm T}$), such as Standard Model measurements, searches for new physics, and in the low-$p_{\rm T}$ regime, such as heavy flavour physics.

In this report, several recent CMS results on b-hadron and quarkonia production and properties are discussed. The key elements for the b-physics program are the very large production cross section at the LHC for heavy flavour quarks, the excellent tracking and muon identification capabilities of the CMS detector, in a wide pseudorapidity range, and a very flexible trigger system, capable of collecting data at high luminosity and high pile-up. All

* Presented at the Cracow Epiphany Conference on Advances in Heavy Flavour Physics, Kraków, Poland, January 9–12, 2018.

the dedicated b-physics triggers are based on the presence of two or more muons, which are reconstructed by the high level trigger (HLT) algorithms, with a very low p_{T} threshold. A typical trigger requires a common vertex for the two muons, plus invariant mass selection. In addition, a separation between the interaction point and the muon vertex may be required. The combination of these selections at HLT allows collecting a large dataset of heavy flavour final states [2].

The results described in this paper include single and double quarkonia production, lifetime measurements of several finale states ($B^0 \to J/\psi K^*$, $B^0 \to J/\psi K^0_{\mathrm{S}}$, $B^0_s \to J/\psi\pi\pi$, $B^0_s \to J/\psi\phi$, $\Lambda_b \to J/\psi\Lambda$, and $B^+_c \to J/\psi\pi$), Λ_b polarization, and a search for $X^+(5568) \to B^0_s\pi^+$. Finally, the rare decays $B^0_{s,d} \to \mu\mu$ and recent measurements of some angular parameters of the $b \to s\ell\ell$ decay $B^0 \to K^*\mu\mu$ will be reviewed.

2. Quarkonia production

2.1. Single quarkonium production

The production of quarkonium in hadronic collisions has been studied by many experiments since the discovery of heavy-quark bound states. The theoretical description is based on Non-Relativistic QCD (NRQCD), which assumes factorization between the perturbative process of creation of a $Q\bar{Q}$ pair, and the following hadronization producing the bound state.

At CMS, a measurement of the double differential production cross section, as a function of pseudorapidity (η) and p_{T}, has been performed for five different final states: J/ψ, $\psi(2S)$, and $\Upsilon(1S, 2S, 3S)$, decaying into a pair of muons. The used datasets correspond to $\mathcal{L} = 2.4$–2.7 fb^{-1}, collected at a center-of-mass energy of 13 TeV [3]. The comparison with a similar measurement done at 7 TeV [4] allows testing the factorization hypothesis. In addition, the extended p_{T} reach at 13 TeV together with the improved statistical precision allows for a better comparison with theoretical calculations. Cross sections of different quarkonium states are calculated in several bins of p_{T} and rapidity $|y|$, in the range of $|y_{\mu\mu}| < 1.2$, according to the formula

$$\frac{\mathrm{d}^2\sigma}{\mathrm{d}p_{\mathrm{T}}\mathrm{d}y}\,\mathcal{B}(q\bar{q} \to \mu\mu) = \frac{N^{(q\bar{q})}(p_{\mathrm{T}}, y)}{\mathcal{L}\Delta p_{\mathrm{T}}\Delta y}\left\langle \frac{1}{(\varepsilon\mathcal{A})(p_{\mathrm{T}}, y)} \right\rangle, \tag{1}$$

where $\mathcal{B}$ is the branching fraction into muons, N is the number of prompt signal events in a bin of width $\Delta p_{\mathrm{T}}, \Delta y$, and $\varepsilon\mathcal{A}$ is the efficiency times acceptance as a function of (p_{T}, y), averaged in each bin. The efficiency takes into account the single muon efficiency, extracted from data with a tag and probe technique, as well as a correction for the presence of two muons. The

number of events is extracted via an unbinned maximum likelihood (UML) fit to the two-muon invariant mass distribution. In the case of $\psi(2S)$ and $\psi(2S)$, also the decay length $c\tau$ is used in the UML fit to separate the prompt and non-prompt components. The analysis does not distinguish feed-down quarkonia from the decay of heavier states.

The comparison with theory predictions is presented in Fig. 1: the predictions for J/ψ are slightly underestimated, and those for $\psi(2S)$ are slightly overestimated; in either case, the disagreement is within the theoretical uncertainties. The theoretical predictions for $\Upsilon(1S, 2S, 3S)$ agree well with data. In the same plot, also the ratio of cross section *versus* p_{T} of 13 TeV measurements and 7 TeV ones is displayed, showing a ratio of about 2–3 for all five final states, with a slow growth as a function of p_{T}, as expected from the evolution of parton density functions at the two center-of-mass energies.

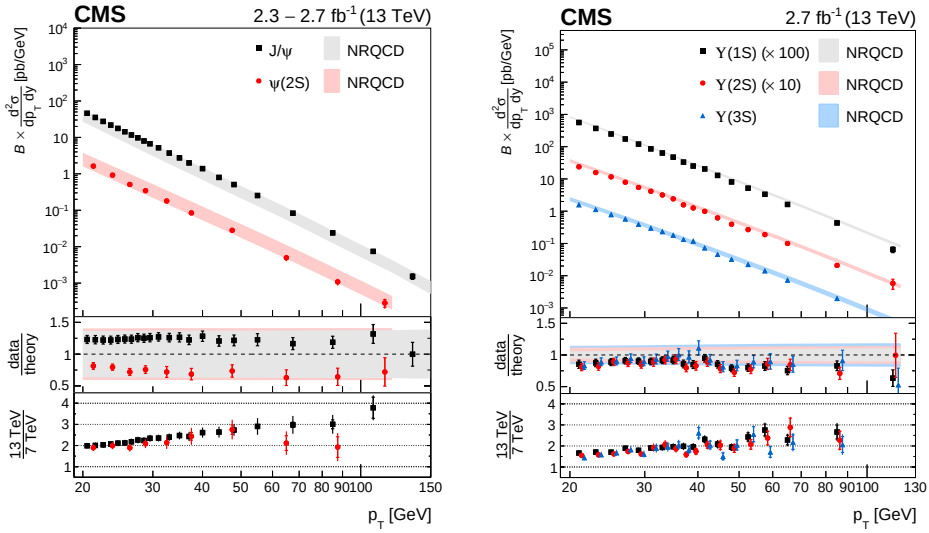


Fig. 1. Comparison of measured single quarkonia cross sections as a function of p_{T} for the five different quarkonia analyzed. The color bands are the predictions from non-relativistic QCD. The bottom plots show the ratios of data to predictions, and between data at 13 and 7 TeV [3].

2.2. Prompt double Υ observation

In addition to the study of single quarkonia production, CMS has also searched for double prompt quarkonia. The observation of double $\Upsilon(1S)$ has been obtained using data collected at 8 TeV, corresponding to an integrated luminosity of $\mathcal{L} = 20.7$ fb^{-1}. This is the first observation of such a production [5].

In the LHC collisions, the composite nature of the colliding protons is such that the primary interactions might occur via single parton–parton collisions (SPS) or multiple distinct interactions, the simplest being double-parton scattering (DPS). Cross-section measurements of quarkonium pair production are crucial to understand SPS and DPS contributions and the parton structure of the proton. At the LHC, given the large parton flux and the high energy, DPS is expected to have a larger contribution [6].

The event selection requires three muons at the high level trigger, with at least one pair of oppositely charged ones with $8.5 < M_{\mu\mu} < 11$ GeV, coming from a common vertex. Four muons with total charge 0 are then requested offline, with $p_{\mathrm{T}} > 3.5$ GeV and $|\eta| < 2.4$. The two pairs of oppositely charged muons are fitted to a common vertex, building two Υ candidates, which must be in the fiducial region $|\eta(\Upsilon)| < 2.0$. Background is mostly coming from miscombined muons from Drell–Yan production, and

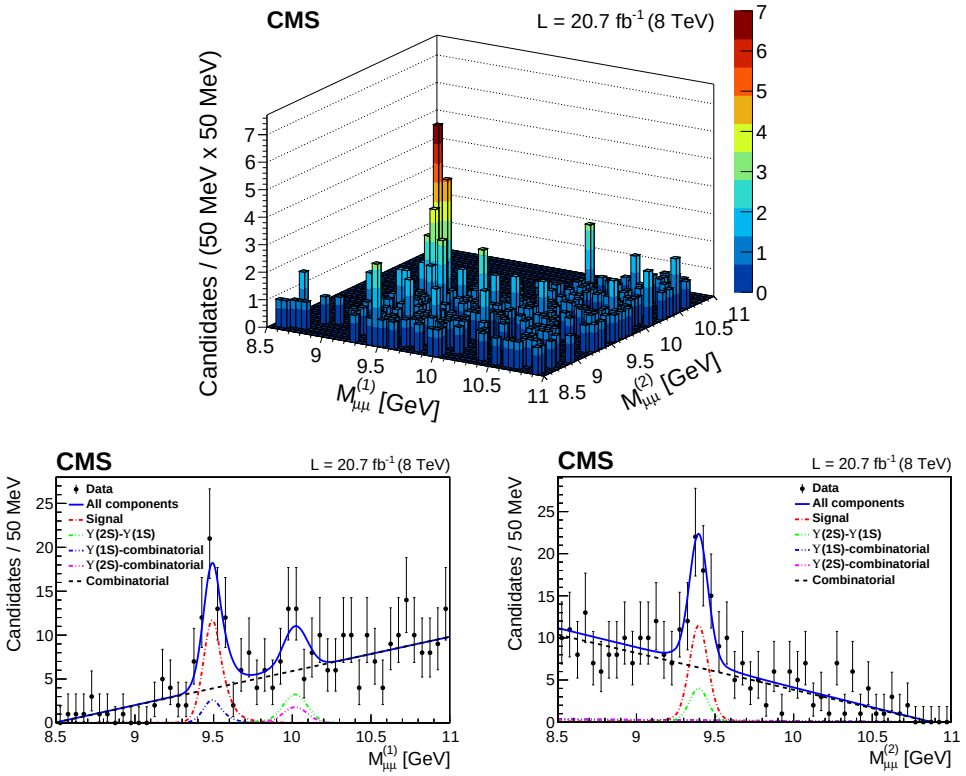


Fig. 2. Di-muon invariant mass distribution for the first (second) muon pair, defined such that $M^{(1)}_{\mu\mu} > M^{(2)}_{\mu\mu}$. The 2D distribution is shown on top, and the two projections with the results of the UML fit superimposed on the bottom. A clear signal of double $\Upsilon(1S)$ is visible, as well as a hint of $\Upsilon(1S)$ $\Upsilon(2S)$ [5].

semileptonic b decay. The signal yield is extracted with a two-dimensional UML fit to the two dimuon invariant masses, including the signal as well as background from various sources: one genuine $\Upsilon(1S)/\Upsilon(2S)$ plus combinatorial or fully combinatorial. Results of the fit are shown in Fig. 2. A total of 38 ± 7 di-Υ events are found, with a large significance ($> 5\sigma$), as well as 13^{+6}_{-5} $\Upsilon(1S)\Upsilon(2S)$ candidates (with a significance of 2.6σ). The fiducial cross section, assuming that both Υ decay isotropically, is found to be $\sigma_{\text{fid}} = 68.8 \pm 12.7(\text{stat.}) \pm 7.4(\text{syst.}) \pm 2.8(\mathcal{B})$ pb. Different hypotheses on polarization change the results, up to $(+36/-38)\%$ for the two extreme cases with a polar anisotropic parameter [7] λ_θ equal to $(+1, +1)$ or $(-1, -1)$, respectively.

These processes are commonly described by an effective cross section (σ_{eff}) that describes the transverse area of the hard partonic interaction [8]. It is estimated as $\sigma_{\text{eff}} = \frac{1}{2}\frac{\sigma^2_{\Upsilon(1S)}}{\sigma_{\text{DPS}}} = \frac{1}{2}\frac{\sigma^2_{\Upsilon(1S)}}{f_{\text{DPS}}\sigma_{\text{fid}}\mathcal{B}^2_{\Upsilon(1S)\to\mu\mu}}$, where $\sigma_{\Upsilon(1S)}$ is the SPS cross section, f_{DPS} is the fraction of the DPS contribution, and $\mathcal{B}$ is the branching fraction of $\Upsilon(1S) \to \mu\mu$. The resulting effective cross section is found to be in the range of $2.2 < \sigma_{\text{eff}} < 6.6$ mb, corresponding to $f_{\text{DPS}} \approx$ 10–30%. This result is in agreement with heavy-quarkonium measurements (2–8 mb) [9], but smaller than that from multi-jet studies 12–20 mb [10]. This might indicate that the mean distance between gluons in the proton (as in quarkonia) is smaller than that between quarks or quark and gluon, which dominates the jet-related channels.

3. Properties

3.1. Lifetime measurements

Precise lifetime measurements involving the weak interaction play an important role in the study of non-perturbative aspects of quantum chromodynamics (QCD). The decays are described with a heavy-quark expansion model, and predictions for the ratios of lifetimes for b hadrons are available.

The lifetime of several b hadrons has been measured by CMS [11], using a dataset of pp collision at 8 TeV, with integrated luminosity of 19.7 fb^{-1}. All these decays include a $J/\psi \to \mu\mu$ in the final states, which is used for triggering. The decays considered are: $B^0 \to J/\psi K^*$, $J/\psi K^0_{\text{S}}$, $B^0_s \to J/\psi\pi\pi$, $J/\psi\phi$, and $\Lambda_b \to J/\psi\Lambda$. Finally, also the decay of $B^+_c \to J/\psi\pi$ has been measured. The weak decay of B^+_c is of particular interest, since it can occur through either b or c quark decay, with the other quark as spectator, or via an annihilation process. Precise measurements can test the complex decay model, and also help to resolve the disagreement between CDF and DØ [12, 13] results and the more recent LHCb [14, 15] one.

The method exploited in the analysis uses the measurement of the proper decay length in the transverse plane: $ct = \frac{L}{(\beta\gamma c)} = \frac{L_{xy}}{(\beta\gamma)_{\mathrm{T}}} = L_{xy}\frac{M}{p_{\mathrm{T}}}$, where $L(L_{xy})$ is the (transverse) decay length, M is the mass of the b hadron, and $p(p_{\mathrm{T}})$ its (transverse) momentum. The lifetime measurement is extracted via a UML fit to the decay length and the invariant mass, taking into account the distortion due to the efficiency, as well as event-per-event uncertainties on the decay length itself. In order to reduce the impact on the turn-on of the efficiency close to $ct = 0$, only the region with $ct > 200$ μm is used for the fit (> 100 μm for the B_c^+ decay).

A single exponential is used for B^0, since the lifetime difference of the light and heavy mass eigenstates is small $\Delta\Gamma_d/\Gamma_d = (-0.3 \pm 1.5)\%$. This is not the case for B_s^0 for which $\Delta\Gamma_s/\Gamma_s = (12.4 \pm 1.1)\%$ [16]. The two final states considered for B_s^0 have very different fractions of light/heavy states. In particular, the decay $J/\psi\pi\pi$ is dominated by the resonant decay $B_s^0 \to J/\psi f(980)$, which is CP-odd. So the lifetime measured in this case corresponds to that of the heavy state τ_{H}, neglecting CP violation in mixing. The other decay mode, $B_s^0 \to J/\psi\phi$, is a mixture of CP-odd and CP-even states, and so an effective lifetime τ_{eff} is actually measured.

The case of B_c^+ decay, which has a shorter lifetime and larger background, is treated in a different way, using a technique previously used by LHCb [15]. The fit is performed on the invariant mass and the ratio of distributions of decay lengths of the considered final state ($B_c^+ \to J/\psi\pi^+$) and that of a large reference sample $B^+ \to J/\psi K^+$. The lifetime of this latter channel has been measured by CMS: $c\tau(B^+) = 490 \pm 0.8(\mathrm{stat.})$ μm, and found in a good agreement with world average value: 491.4 ± 1.2 μm [16]. In the ratio, the resolution function — $G(ct)$ — which convolves the exponential has been verified, with simulated pseudo-events, to cancel out, reducing the ratio to

$$\mathcal{R}(ct) = \frac{N_{B_c^+}}{N_{B^+}} = \frac{e^{-t/\tau_{B_c^+}} \otimes G(ct)}{e^{-t/\tau_{B^+}} \otimes G(ct)} \frac{\varepsilon_{B_c^+}}{\varepsilon_{B^+}} \approx \mathcal{R}_\varepsilon(ct) e^{-\Delta\Gamma t}\,, \tag{2}$$

where $\Delta\Gamma = 1/\tau_{B_c^+} - 1/\tau_{B^+}$ and $\mathcal{R}_\varepsilon(t)$ is the ratio of the efficiencies as a function of the decay length for the two channels. The quantity $\Delta\Gamma$ is extracted via a binned χ^2 fit to the $\mathcal{R}(ct)$ distribution, corrected for the efficiency ratio, with an exponential function. Finally, using the world average τ_{B^+}, the result for $c\tau_{B_c^+}$ is obtained.

The results of the measurements are the following:

$$
\begin{aligned}
c\tau_{B^0\to J/\psi K^*} &= 453.0 \pm 1.6(\text{stat.}) \pm 1.5(\text{syst.})\ \mu\text{m}\,,\\
c\tau_{B^0\to J/\psi K^0_S} &= 457.8 \pm 2.7(\text{stat.}) \pm 2.7(\text{syst.})\ \mu\text{m}\,,\\
c\tau_{B^0_s\to J/\psi\pi^+\pi^-} = c\tau_{\text{H}} &= 502.7 \pm 10.2(\text{stat.}) \pm 3.2(\text{syst.})\ \mu\text{m}\,,\\
c\tau_{B^0_s\to J/\psi\phi} &= 443.9 \pm 2.0(\text{stat.}) \pm 1.2(\text{syst.})\ \mu\text{m}\,,\\
c\tau_{\Lambda_b} &= 442.9 \pm 8.2(\text{stat.}) \pm 2.7(\text{syst.})\ \mu\text{m}\,,\\
c\tau_{B_c^+} &= 162.3 \pm 8.2(\text{stat.}) \pm 4.4(\text{syst.}) \pm 0.1(\tau_{B^+})\ \mu\text{m}\,.
\end{aligned}
$$

Combining the two results for B_s^0, and using the world average CP-odd amplitude $|A_\perp|^2 = 0.250 \pm 0.006$ [16], it is possible to extract the lifetime for the light eigenstate $c\tau_{\text{L}} = 420.4 \pm 6.1\ \mu$m.

All the results are in a good agreement with the world average values. The result for B_c^+ confirms an higher lifetime value than that measured at Tevatron ($135.5 \pm 9.6\ \mu$m) [12, 13], which is in a good agreement with LHCb [14].

3.2. Λ_b polarization

The decay $\Lambda_b \to J/\psi(\to \mu\mu)\Lambda(\to p\pi^-)$ is a rich source of information about the effect of strong interactions in hadronic decays. From an angular analysis of the decay, it is possible to measure many parameters, including polarization P, the parity-violating decay asymmetry α_1, and the longitudinal polarization of Λ, α_2 [17].

The analysis [18] uses data collected at 7 and 8 TeV, with an integrated luminosity of 5.2 and 19.8 fb^{-1}, respectively. The decay can be fully described by five angles, but can be reduced to three assuming uniform detector acceptance over the azimuthal ones. The signal is extracted in four categories, at 7(8) TeV, and for Λ_b and $\bar{\Lambda}_b$. About five thousand events in total are collected in all the categories. The angular variables $\theta_L, \theta_p, \theta_\mu$ as well as the invariant mass are fitted with an UML fit to extract the physical parameters, as shown in Fig. 3.

The final results are: $P = 0.00 \pm 0.06(\text{stat.}) \pm 0.06(\text{syst.})$, $\alpha_1 = 0.14 \pm 0.14(\text{stat.}) \pm 0.10(\text{syst.})$, and $\alpha_2 = -1.11 \pm 0.04(\text{stat.}) \pm 0.05(\text{syst.})$, in a good agreement with previous measurements [19]. The polarization result favours the perturbative QCD prediction (10%) [20], while disfavours a model with larger P [21]. The α_1 value disfavours the HQET prediction [21], while α_2 agrees with the predicted negative helicity for Λ.

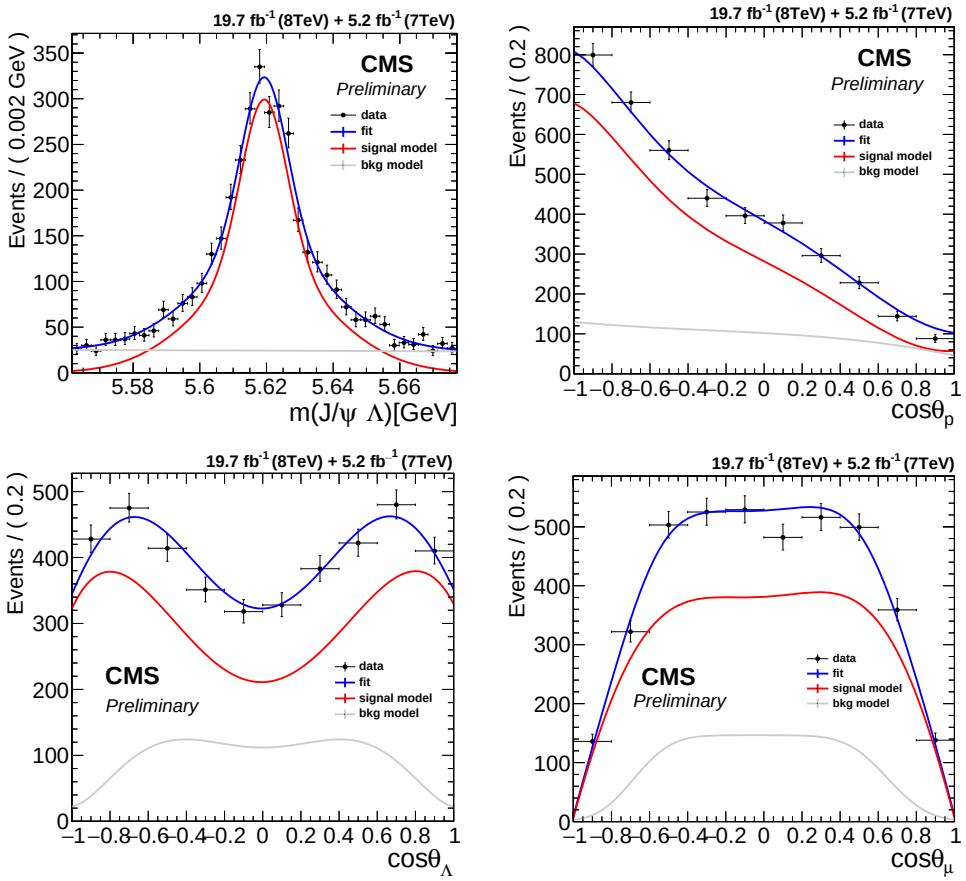


Fig. 3. Distributions of invariant mass and angular variables in the decay of Λ_b, together with the results of the UML fit, showing the signal as well as background models [18].

4. Spectroscopy

4.1. Search for $X^+(5568) \to B_s^0\pi^+$

A search for resonance in the decay of $B_s^0\pi^+$ has been performed with data collected at 8 TeV, $\mathcal{L} = 19.7$ fb^{-1} [22], triggered by the observation by D$\emptyset$ of a resonance $X^+(5568)$ [23] with large statistical significance, subsequently not confirmed by LHCb [24].

The CMS dataset comprises about ~50 000 $B_s^0 \to J/\psi\phi$ decays. An additional π^+ with $p_T > 0.5$ GeV is added, without any requirement on $\Delta R(B_s^0, \pi)$ for separation between the two decay products, as was instead done by D$\emptyset$. A scan of the five-body invariant mass has been performed,

confronting the B_s^0 signal region and the side bands, as shown in Fig. 4. No resonance-like structure is visible, and an upper limit has been set for the relative production of $X(5568)$ *versus* B_s^0: $\rho_x < 1.1\%$ at 90% C.L., to be compared with the D$\emptyset$ result of $\rho_x(\mathrm{D}\emptyset) = 8.6 \pm 2.6(\mathrm{stat.}) \pm 1.6(\mathrm{syst.})\%$. The limit depends very mildly on the width of the resonance. It is worth to note that an additional selection on ΔR strongly affects the invariant mass distribution, as shown in Fig. 4, with a more important effect on the B_s^0 signal region with respect to the sidebands.

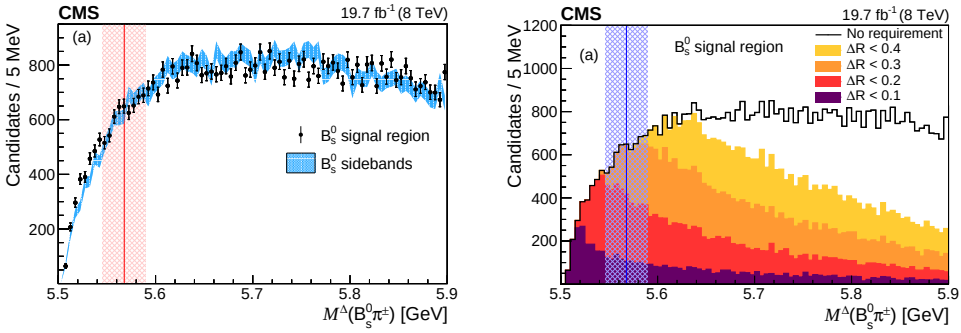


Fig. 4. Invariant mass distribution of the $B_s^0\pi^+$ system, superimposed to the same distribution for candidates in the B_s^0 sidebands (left). Effect of applying a ΔR selection on the sample (right) [22].

5. Rare decays and angular analysis

5.1. Observation of the $B_s^0 \to \mu\mu$ decay

The search for $B_s^0/B^0 \to \mu\mu$ has been performed by CMS at $\sqrt{s} = 7(8)$ TeV, with $\mathcal{L} = 5(20)$ fb^{-1} [25]. The signal is characterized by two muons from one well-reconstructed secondary B vertex, with the dimuon momentum aligned with the flight direction, the dimuon mass around the B mass, and isolated dimuons. The background has different components: the combinatorial one, estimated from data side bands; from rare B decays ($B_s^0 \to K^-\mu\nu$, $\Lambda_b \to p\mu\nu$) estimated from simulated events; and peaking ($B^0 \to KK, K\pi, \pi\pi$) whose absolute yield is evaluated with an independent single-μ trigger. The signal selection is based on strict requirements for muon identification quality, using an MVA technique, good secondary vertex reconstruction, an isolation requirement with respect to other tracks in the event, and a selection on the B pointing angle. The excellent muon identification and resolution of the CMS detector allow for a powerful background rejection in the $M_{\mu\mu}$ invariant mass distribution.

The $B^{\pm} \to J/\psi K^{\pm} \to \mu\mu K^{\pm}$ decay is used as a normalization channel, taking into account the acceptance, trigger, and reconstruction efficiencies, as well as the B-fragmentation fraction ratio f_s/f_u [26]. The B^0 and B_s^0 yields are extracted via a UML fit using several categories of events based on the data-taking period and the event classification.

The results are shown in Fig. 5. The branching fractions for the two decays are the following: $\mathcal{B}(B_s^0 \to \mu\mu) = \left(3.0^{+0.9}_{-0.8}(\text{stat.})^{+0.6}_{-0.4}(\text{syst.})\right) \times 10^{-9}$ and $\mathcal{B}(B_d^0 \to \mu\mu) = \left(3.5^{+2.1}_{-1.8}(\text{stat.} + \text{syst.})\right) \times 10^{-10}$. The observed significance is 4.3 and 2.0σ, respectively. Given the low significance of the B_d^0 decay, an upper limit of $\mathcal{B}(B_d^0 \to \mu\mu) < 1.1 \times 10^{-9}$ at 95% C.L. is set.

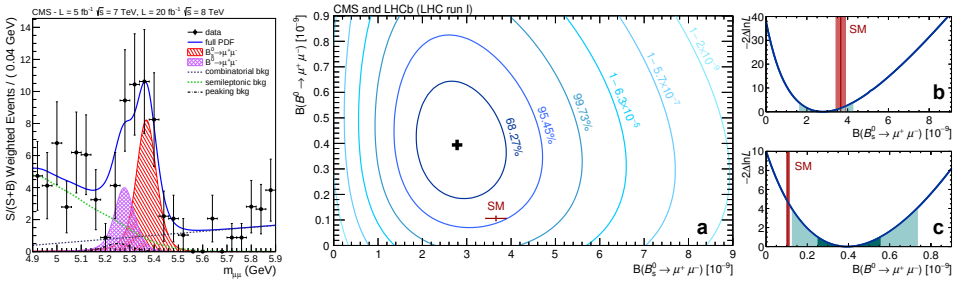


Fig. 5. (Left) Di-muon invariant mass for the combination of all CMS categories [25]. Individual categories are weighted with $S/(S+B)$, where $S(B)$ is the signal (background) determined at the B^0 peak position. (Right) Combined results for CMS and LHCb for $\mathcal{B}(B_s^0/B_d^0)$ compared with the SM prediction [27].

A combined analysis [27] of CMS and LHCb [28] provides the following results: $\mathcal{B}(B_s^0 \to \mu\mu) = (2.8^{+0.7}_{-0.6}) \times 10^{-9}$ and $\mathcal{B}(B_d^0 \to \mu\mu) = (3.9^{+1.6}_{-1.4}) \times 10^{-10}$, with a combined significance of 6.2 (7.4 expected) and 3.2σ (0.8 exp.).

5.2. Angular analysis of $B^0 \to K^*\mu\mu \to K^+\pi^-\mu^+\mu^-$

The FCNC decay $B^0 \to K^*\mu\mu \to K^+\pi^-\mu^+\mu^-$ has a four-body, fully charged final state that can be fully reconstructed. The decay topology is described by three angles $\theta_\ell, \theta_K, \varphi$, depicted in Fig. 6, and the dimuon invariant mass squared $q^2 = M^2_{\mu\mu}$. The initial state B^0 ($\bar{B}^0$) can be identified via K and π charges.

For several parameters of the angular distribution, robust SM predictions are available: some of these parameters have been measured by CMS [29], including the forward–backward asymmetry of the muons, A_{FB}, the longitudinal polarization fraction of the K^*, F_{L}, and the branching fraction as a function of q^2, $\mathrm{d}B/\mathrm{d}q^2$, in a good agreement with SM predictions. The same dataset has been reused to determine the two parameters P_5' and

P_1 [30], which are combinations of Wilson coefficients of the effective Hamiltonian [31]. In this analysis, seven bins of q^2 have been used, in the range of 1 to 19 GeV^2.

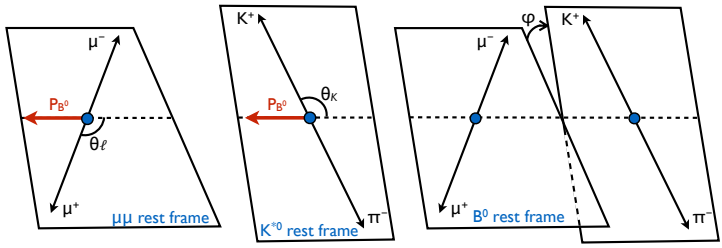


Fig. 6. Sketch of the decay $B^0 \to K^*\mu\mu \to K^+\pi^-\mu^+\mu^-$ with the definition of the three angles describing the final state: $\theta_\ell, \theta_K, \varphi$ [30].

Events are selected with a trigger requiring two oppositely charged muons from a displaced vertex, with $p_\text{T} > 3.5$ GeV and $|\eta| < 2.2$, $p_\text{T}^{\mu\mu} > 6.5$ GeV, and with the line of flight aligned with the dimuon momentum: $\cos\alpha > 0.9$. Offline reconstruction repeats the trigger requirements, and requires two oppositely charged hadrons, with $p_\text{T} > 0.8$ GeV, displaced with respect to the beamspot, and with $|M_{K\pi} - M_{K^*}| < 90$ MeV, where both mass hypotheses are used for each track, and a stricter cut on $\cos\alpha$. An additional selection $M_{KK} > 1.035$ MeV is added, to reduce ϕ contamination. The B^0 candidate is reconstructed by fitting the four tracks to a common vertex. It is required to have $p_\text{T} > 8$ GeV, $|\eta| < 2.2$, displaced from the beamspot, with the momentum pointing to the beamspot, and $|M - M_{B^0}| < 280$ MeV. The B^0 flavour is determined depending on which of the $K^\pm\pi^\mp$ invariant masses is closest to the nominal K^* one. The mistag probability is estimated from simulation to be 12–14%, depending on q^2.

Two control regions are identified for $B^0 \to J/\psi(\to \mu\mu)K^*$ and ψ', based on the dimuon invariant mass $|q - M_{J/\psi(\psi')}| < 3\sigma_M$. A further diagonal band in the plane (M, q) is vetoed on the low side of the control regions in order to reduce contamination from unreconstructed soft photons in the charmomium decay. After applying these requirements, 3191 events remain.

The signal contributes to the final state with both P-wave and S-wave, as well as interference [36]. The original 14 parameters of the differential decay rate are reduced to six by folding around $\varphi = 0$ and $\theta_\ell = \pi/2$. Furthermore, three parameters, F_L, F_S, and A_s, are fixed from the previous measurement, and A_s^5 is treated as a nuisance parameter, leaving only P_1 and P_5' to be measured.

The full probability density function (pdf) has contributions also from mistagged events, as well as from background ones. In order to tell apart signal and background, the B^0 invariant mass is also included in the pdf,

modelled with a double Gaussians with common mean. The complete unnormalized pdf $(m, \cos\theta_K, \cos\theta_l, \phi)$ for each bin in q^2 is shown in Eq. (3)

$$\begin{aligned}\text{pdf} \;=\; & Y_{\mathrm{S}}^{\mathrm{C}} \left(S_i^{\mathrm{R}}(m)\, S_i^a(\cos\theta_K, \cos\theta_l, \phi)\, \epsilon_i^{\mathrm{R}}(\cos\theta_K, \cos\theta_l, \phi) \right. \\ & + \frac{f_i^{\mathrm{M}}}{1 - f_i^{\mathrm{M}}}\; S_i^{\mathrm{M}}(m)\, S_i^a(-\cos\theta_K, -\cos\theta_l, -\phi)\, \epsilon_i^{\mathrm{M}}(\cos\theta_K, \cos\theta_l, \phi) \Big) \\ & + Y_{\mathrm{B}}\, B_i^m(m)\, B_i^{\cos\theta_K}(\cos\theta_K)\, B_i^{\cos\theta_l}(\cos\theta_l)\, B_i^{\phi}(\phi)\,, \end{aligned} \tag{3}$$

where S_i^a is the pdf for signal, $Y_{\mathrm{S}}^{\mathrm{C}}$ and Y_{B} are the signal and background yield, respectively, and f_i^{M} is the mistag fraction. The background is evaluated from data side bands, found to be factorizable, and modelled as second- to fourth-order polynomial. The efficiencies $\epsilon_i^{\mathrm{R/M}}(\cos\theta_K, \cos\theta_l, \phi)$ are evaluated from simulated events separately for correctly tagged and mistagged events as a function of the three angles.

An extended UML fit is performed on data, in each bin of q^2, in two steps. First, the background pdf are determined by fitting the invariant mass side bands. These pdf are then fixed for the second step, where a fit on the full mass range is performed. This second step is performed by discretizing the P_1, P_5' space, maximizing the likelihood $\mathcal{L}$ as a function of the three remaining nuisance parameters $Y_{\mathrm{S}}^{\mathrm{C}}$, Y_{B}, and A_5^s, and finally fitting the $\mathcal{L}$ with a bivariate Gaussian in order to find the absolute maximum inside the physical domain, where the pdf is always positively defined. The statistical uncertainties of the results are evaluated using the profiled Feldman–Cousins method [32] with nuisance parameters.

Systematic uncertainties include effects from simulation mis-modeling, fit bias, limited amounts of simulated data, efficiency shape, mistag probability, background distribution, mass distribution, angular resolution effects, and feed-through background from control regions. These are evaluated from a large sample simulated events, pseudo-experiment constructed combining the simulated signal with background from data side bands, fit on control regions, and propagation, via pseudo-experiments, of other uncertainties.

An important systematic uncertainty is due to the usage of fixed values of F_L, F_S, and A_s from previous measurements on the same dataset. This has been evaluated via pseudo-experiments with sample larger than data, by comparing a full fit with the three parameters fixed and free to float. No bias has been found, and the comparison of the statistical uncertainties on P_1 and P_5' in the two fits are used to assign the systematics uncertainties.

The final signal yield in all seven bins is 1397 events. The results on P_1 and P_5' are shown in Fig. 7, where also the results published by the LHCb [33] and Belle [34] collaborations are shown. Two SM predictions, denoted SM-DHMV [35, 36] and SM-HEPfit [37], are available for comparison with the measured angular parameters. The second prediction uses LHCb data [33]

to obtain the hadronic contribution. Both sets of predictions are seen to be in agreement with the CMS results, although the agreement with the SM-DHMV prediction is somewhat better. Thus, we do not obtain evidence for physics beyond the SM. Qualitatively, the CMS measurements are compatible with the LHCb results. The Belle measurements lie systematically above both the CMS and LHCb results and the SM predictions.

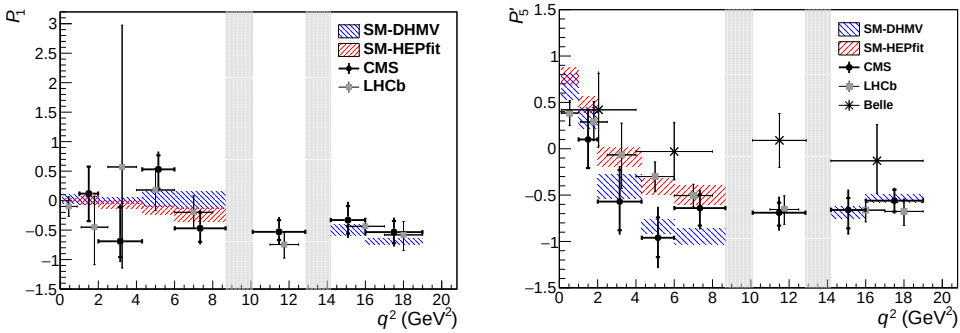


Fig. 7. CMS measurements of the P_1 and P_5' angular variables *versus* q^2 for $B^0 \to K^*\mu\mu$ decays, in comparison to the results from the LHCb [33] and Belle [34] collaborations. The statistical uncertainties are shown by the inner vertical bars, while the outer vertical bars give the total uncertainties. The horizontal bars show the bin widths. The vertical shaded regions correspond to the J/ψ and ψ' resonances. The hatched regions show the predictions from the two SM calculations described in the text, averaged over each q^2 bin.

6. Summary

Several measurements in the field of heavy flavour physics, performed by CMS at 7, 8, and 13 TeV center-of-mass energies have been presented. The results are generally in agreement with Standard Model predictions, and prove the capability of the CMS detector to provide precise measurements for processes involving b quarks.

REFERENCES

[1] CMS Collaboration, *JINST* **3**, S08004 (2008).

[2] CMS Collaboration, Heavy Flavour Distributions from CMS with 2017 Data at $\sqrt{s} = 13$ TeV, Technical Report, Jul 2017 CMS-DP-2017-029.

[3] CMS Collaboration, *Phys. Lett. B* **780**, 251 (2018) [arXiv:1710.11002 [hep-ex]].

[4] CMS Collaboration, *Phys. Rev. Lett.* **114**, 191802 (2015).

[5] CMS Collaboration, *J. High Energy Phys.* **1705**, 013 (2017).

[6] S.P. Baranov, A.M. Snigirev, N.P. Zotov, *Phys. Lett. B* **705**, 116 (2011).
[7] CMS Collaboration, *Phys. Rev. Lett.* **110**, 081802 (2013).
[8] G. Calucci, D. Treleani, *Phys. Rev. D* **60**, 054023 (1999).
[9] DØ Collaboration, *Phys. Rev. D* **90**, 111101 (2014).
[10] CMS Collaboration, *J. High Energy Phys.* **1403**, 032 (2014).
[11] CMS Collaboration, *Eur. Phys. J. C* **78**, 457 (2018) [arXiv:1710.08949 [hep-ex]].
[12] DØ Collaboration, *Phys. Rev. Lett.* **102**, 092001 (2009).
[13] CDF Collaboration, *Phys. Rev. D* **87**, 011101 (2013).
[14] LHCb Collaboration, *Eur. Phys. J. C* **74**, 2839 (2014).
[15] LHCb Collaboration, *Phys. Lett. B* **742**, 29 (2015).
[16] C. Patrignani *et al.* [Particle Data Group], *Chin. Phys. C* **40**, 100001 (2016).
[17] M. Krämer, H. Simma, *Nucl. Phys. B Proc. Suppl.* **50**, 125 (1996).
[18] CMS Collaboration, *Phys. Rev. D* **97**, 072010 (2018) [arXiv:1802.04867 [hep-ex]].
[19] LHCb Collaboration, *Phys. Lett. B* **724**, 27 (2013).
[20] G. Hiller, M. Knecht, F. Legger, T. Schietinger, *Phys. Lett. B* **649**, 152 (2007).
[21] Z.J. Ajaltouni, E. Conte, O. Leitner, *Phys. Lett. B* **614**, 165 (2005).
[22] CMS Collaboration, *Phys. Rev. Lett.* **120**, 202005 (2018) [arXiv:1712.06144 [hep-ex]].
[23] DØ Collaboration, *Phys. Rev. Lett.* **117**, 022003 (2016).
[24] LHCb Collaboration, *Phys. Rev. Lett.* **117**, 152003 (2016).
[25] CMS Collaboration, *Phys. Rev. Lett.* **111**, 101804 (2013).
[26] LHCb Collaboration, *J. High Energy Phys.* **1304**, 1 (2013).
[27] LHCb and CMS collaborations, *Nature* **522**, 68 (2015).
[28] LHCb Collaboration, *Phys. Rev. Lett.* **111**, 101805 (2013).
[29] CMS Collaboration, *Phys. Lett. B* **753**, 424 (2016).
[30] CMS Collaboration, *Phys. Lett. B* **781**, 517 (2018) [arXiv:1710.02846 [hep-ex]].
[31] J. Matias, F. Mescia, M. Ramon, J. Virto, *J. High Energy Phys.* **1204**, 104 (2012).
[32] G.J. Feldman, R.D. Cousins, *Phys. Rev. D* **57**, 3873 (1998).
[33] LHCb Collaboration, *J. High Energy Phys.* **1602**, 104 (2016).
[34] Belle Collaboration, *Phys. Rev. Lett.* **118**, 111801 (2017) [arXiv:1612.05014 [hep-ex]].
[35] S. Descotes-Genon, J. Matias, M. Ramon, J. Virto, *J. High Energy Phys.* **1301**, 048 (2013).
[36] S. Descotes-Genon, T. Hurth, J. Matias, J. Virto, *J. High Energy Phys.* **1305**, 137 (2013).
[37] M. Ciuchini *et al.*, *J. High Energy Phys.* **1606**, 116 (2016).